Research Square

Preprints are preliminary reports that have not undergone peer review.
They should not be considered conclusive, used to inform clinical practice,
or referenced by the media as validated information.

Interindividual variations in methane production in tree trunks in relation to the wood micro-environment and microbial communities

Nathan Cousteur
Université de Lorraine, AgroParisTech, INRAE, UMR Silva
Takumi Mochidome
Graduate School of Agriculture, Kyoto University
Takeshi Watanabe
Graduate School of Bioagricultural Sciences, Nagoya University
Susumu Asakawa
Graduate School of Bioagricultural Sciences, Nagoya University
Shunsuke Matsuoka
Graduate School of Agriculture, Kyoto University
Masako Dannoura
Graduate School of Agriculture, Kyoto University
Dorine Desalme
Université de Lorraine, AgroParisTech, INRAE, UMR Silva
Caroline Plain
Université de Lorraine, AgroParisTech, INRAE, UMR Silva
Daniel Epron
daniel.epron.3a@kyoto-u.ac.jp

Graduate School of Agriculture, Kyoto University

Research Article

Keywords: Heartwood, methanogenesis, living trees, wood degradation

Posted Date: November 13th, 2026

DOI: https://doi.org/10.21203/rs.3.rs-11398257/v1

License: This work is licensed under a Creative Commons Attribution 4.0 International License.
Read Full License

Additional Declarations: No competing interests reported.

Title: Interindividual variations in methane production in tree trunks in relation to the wood micro-environment and microbial communities

Authors: *Nathan Cousteur[1,2], Takumi Mochidome[2], Takeshi Watanabe[3], Susumu Asakawa[3], Shunsuke Matsuoka[2], Masako Dannoura[2], Dorine Desalme[1], Caroline Plain[1], Daniel Epron[2]*

[1]*Université de Lorraine, AgroParisTech, INRAE, UMR Silva, F54000 NANCY, France*

[2]*Graduate School of Agriculture, Kyoto University, Kyoto, Kyoto Prefecture, 606-8224, Japan*

[3]Graduate School of Bioagricultural Sciences, Nagoya University, Nagoya, Aichi Prefecture, 464-0814, Japan

ORCID

NC: 0009-0006-8792-109X
TM: 0009-0001-1034-8575
TW: 0000-0002-1736-0585
SA: 0000-0002-5878-0674
SM: 0000-0002-3723-8800
MD: 0000-0003-0389-871X
DD: 0000-0002-2403-3435
CP: 0000-0002-3624-1127
DE: 0000-0001-9451-3437

Corresponding authors
Daniel Epron (daniel.epron.3a@kyoto-u.ac.jp)
Nathan Cousteur (nathan.cousteur@laposte.net)

Summary

Key message: Methane accumulates in the heartwood of two tree species independently of the presence of wetwood. Moisture or density drives anoxia, while species-specific microbial communities and early decay stages might promote methanogenesis.

Methane (CH_4) accounts for approximately 20% of global warming. Recent evidence suggests that CH_4 accumulating in living tree trunks of some species can be produced internally by methanogenic archaea, yet the factors governing microbial community composition and activity within trunks remain poorly understood. This study characterises the microenvironment conducive to methanogenesis within the heartwood of two contrasting species: *Cryptomeria japonica*, prone to wetwood formation, and *Fagus crenata*, in which this phenomenon remains rare. *In-situ* CH_4 molar fractions, ex-situ potential production rates, physical and biochemical properties, and bacterial community composition were assessed. Elevated CH_4 molar fractions were consistently observed in the heartwood of both species, regardless the presence of wetwood. Anoxic conditions were driven by high moisture content in *C. japonica*, whereas high bulk density promoted oxygen limitation in *F. crenata*. Microbial communities differed markedly between species and among individuals, reflecting variations in methanogenic activity and internal decay state. Temporal dynamics of microbial communities emerged as key drivers of CH_4 production. A non-linear pattern was identified: early-stage wood degradation promotes CH_4 accumulation, whereas advanced degradation limits production.

Key Words: Heartwood, methanogenesis, living trees, wood degradation

Introduction

Trees represent a significant source of uncertainty in global methane (CH_4) budgets, as they can act either as sources or sinks of atmospheric CH_4 (Saunois et al. 2020; Gauci et al. 2024; Epron et al. 2026). Understanding the processes governing CH_4 fluxes from trees in forest ecosytrunks is therefore essential, as their contribution to the global CH_4 budget should not be overlooked.

Trees in wetland forests emit methane produced in flooded, anoxic soils (Pangala et al. 2013, 2015; Terazawa et al. 2015; Jeffrey et al. 2020; Sakabe et al. 2021). Although methane production can also occur in soils of upland forests, particularly in deep, moist soil layers, with emission at the base of trunks (Pitz et al. 2018; Welch et al. 2019; Plain et al. 2019), the methane that accumulates in large, living tree trunks can also be produced within the trunks themselves (Wang et al. 2017; Epron et al. 2023; Mochidome et al. 2025). Methanogens have been detected in the wood of several tree species, where they produce methane through hydrogenotrophic (main pathway), acetoclastic, or methylotrophic pathways under anaerobic conditions (Zeikus and Henning 1975; Yip et al. 2018; Flanagan et al. 2021; Feng et al. 2022; Smits et al. 2022; Harada et al. 2024; Gewirtzman et al. 2025; Arnold et al. 2025; Mochidome et al. 2025). Methane produced in the trunk can accumulate to remarkably high molar fractions, reaching up to 50% of the total gas content in some cases (Wang et al. 2017; Gewirtzman et al. 2025; Mochidome et al. 2025; Epron and Mochidome 2026).

Favourable conditions for methanogenesis and CH_4 production may occur in wetwood-bearing species but potentially in all tree species where oxygen diffusion to the heartwood is limited. Such limitation may arise from low wood porosity associated with high wood density and/or water content (Wang et al. 2017, 2021; Epron et al. 2023). However, the dominant metabolic pathways leading to the production of substrates that fuel methanogenesis remain poorly constrained but could partly explain the large interspecific and intraspecific variability in CH_4 molar fractions that have been measured. This variability suggests that local physicochemical and microenvironmental conditions within the wood may play a determinant role. Indeed, methanogenesis is a highly sensitive process, known to be regulated by a range of environmental parameters including pH, temperature, moisture, and the availability of both substrates and inhibitory compounds (Le Mer and Roger 2001). In living tree trunks, these parameters may vary considerably, both radially and vertically, generating heterogeneous

conditions, for example wood moisture (Nakada, 2006; Nakada et al., 2003), impacting methanogenic activity.

Critical uncertainties remain; it is still unclear which substrates primarily fuel methanogenesis in the wood of living trees; where they come from; and how their availability varies depending on the microenvironment inside the trunk. Although a recent study highlighted a strong correlation between trunk CH_4 fluxes and wood decay severity (Senevirathne et al. 2026), intraspecific variability in CH_4 molar fraction and production has often shown no clear relationship with the presence of rotten wood (Covey et al. 2012; Wang et al. 2017; Barba et al. 2021; Epron and Mochidome 2026). While advanced wood rot can lead to oxygen invasion into woody tissues, thereby inhibiting methanogenesis (Covey et al. 2012; Epron et al. 2023), the onset of wood degradation may be a source of substrates fuelling methanogenesis (Mukhin and Voronin 2007; Epron and Mochidome 2026).

The widespread presence of methanogenic microorganisms within the trunks of living trees further underscores the need to understand how microbial community structure is shaped by local environmental conditions (Arnold et al. 2025). Methanogenic archaea do not operate in isolation but are embedded within complex microbial communities involving syntrophic or symbiotic interactions with fermentative bacteria (Schink and Ward 1984; Demirel and Scherer 2008) whose composition reflects local oxygen availability and substrate pools. Fungal decomposition of wood is another putative source of substrates, and this activity can also alter the oxygenation conditions of wood tissues (Mukhin et al., 2006; Mukhin & Voronin, 2007; Senevirathne et al., 2026). The feedbacks of bacteria and fungi on their environment, through which microbial activity modifies local chemical conditions and in turn shapes community structure, may therefore play an important role in regulating methanogenic activity in tree trunks.

In this study, we aimed to characterise the microenvironment that favours CH_4 production in tree heartwood and to identify the physicochemical and microbial drivers of methanogenic activity. We hypothesised that (i) methane production in wood is primarily localised in the heartwood, where anoxic conditions prevail, independently of wet heartwood presence, but that the level of methanogenic activity is not determined solely by radial localization. Rather, it is further modulated by local physicochemical conditions, including pH, substrate and inhibitor availability, moisture and wood density, that vary independently of the

sapwood/heartwood distinction. We further hypothesised that (ii) variation in methanogenic activity among heartwood wood segments reflects differences in the structure of bacterial and fungal communities, shaped by oxygen availability and reinforced by microbial–environmental feedbacks operating through substrate production.

To test these hypotheses, we measured the molar fractions of CH_4 and CO_2, as well as the potential CH_4 production rates, in the trunks of two contrasting tree species: *Cryptomeria japonica* (Japanese cedar), which frequently exhibits wetwood (moisture content > 100%), and *Fagus crenata* (Japanese beech), which generally does not. We further characterised the physicochemical properties of the wood, and after confirming that methane production was the highest in the heartwood, we analysed the bacterial and fungal communities inhabiting the inner heartwood.

Materials and methods

Study site and trees

The evergreen conifer *Cryptomeria japonica* D. Don and the deciduous broadleaf species *Fagus crenata* Blume were chosen because preliminary experiments identified methanogenic archaea in their trunk (Harada et al. 2024; Mochidome et al. 2025). The sampling was conducted at the Ashiu Forest Research Station of the Field Science Education and Research Centre (Kyoto University) in the northern part of Kyoto prefecture, Japan (35.34 N, 135.76 E) at an altitude of 650 m for *C. japonica* and 745m for *F. crenata*, with a mean annual temperature of 10.3 ºC and annual precipitation of 2,732 mm between 2011 and 2020. The well-drained, slightly acidic soil (pH = 4.5) with a sandy loam texture (68% sand, 22% silt, and 10% clay) acts as a net sink for CH4 (-0.66 g CH_4 ha^{-1} h^{-1}, Paul et al., 2026). The selected trees had a mean diameter of 65 cm ± 1.7 cm (n=8) for *C. japonica* and 46 cm ± 1.1 cm (n=6) for *F. crenata* (Table S1).

Measurement of *in-situ* molar fraction of CH_4 and CO_2

Each tree trunk was cored at a height of 1.3 m using an increment borer (12 mm internal diameter, Haglöf Sweden) at three different depths to reach the inner heartwood (pith), outer heartwood and sapwood in May 2024. The materials were disinfected before collecting a sample. The wood cores were cut into three segments: sapwood (“sw”), outer heartwood (“o”) from nearby the sapwood to the middle of the heartwood and inner heartwood (“i”), from the middle of the heartwood to the pith. It should be noted that for each tree, three samples of sapwood were taken, two samples of outer heartwood, while only one segment of inner heartwood was taken. Each segment was then enclosed in a polyethene bag, from which air was removed as much as possible by hand compression before closure and stored in a cooler box for a maximum of 24 hours. After removing the wood core, a stainless-steel tube (16 mm outer diameter) was inserted into the three holes in each tree, driven by a hammer. The tube was flushed with pure N_2 to expel as much O_2 as possible, then the open end of the tube was capped with a rubber septum (Asone, Butyl W Plug, Osaka, Japan). Additionally, three tubes with an external diameter of 6 mm were inserted in the soil at three different depths (10, 20 and 40 cm) near the investigated trees and closed with a rubber septum too. After at least five days, a gas sample was collected using a syringe from inside each tube by

puncturing its septum. The sampled volume varied from 0.01 ml to 0.2 ml depending on the concentration to stay within the measurement range of the trac gas analyser (Li-7810, Licor; Lincoln, USA; range and precision, 0-100 ppm and 6×10^{-4} ppm at 2 ppm for CH_4; 0-10,000 ppm and 3.5 ppm at 400 ppm for CO_2). The gas sample was promptly injected into a small volume sample kit (Li 7810-110), which was connected to the gas analyser. Before each injection, both the analyser and the sampling kit were purged with ambient air. The molar fractions of CH_4 and CO_2 in the injected gas samples (CH_{4S} and CO_{2S}) were determined using the following eqaution:

$$\mathrm{CH}_{4S} = \frac{V_L \times (\mathrm{CH}_{4P} - \mathrm{CH}_{4B}) + V_S \times \mathrm{CH}_{4P}}{V_S} \quad [1]$$

where V_L is the volume of the sytrunk (sample kit and analyser), V_S is the injected volume, CH_{4B} and CH_{4P} are the molar fractions in the closed loop before and after injection (Mochidome and Epron 2024). CO_{2S} was calculated similarly, using CO_{2B} and CO_{2P} instead of CH_{4B} and CH_{4P}.

Estimation of *ex-situ* potential CH_4 production rate

The methanogenic activity in the wood segments was assessed within 24 hours after coring the trees. For each tree, three to five pieces of 4 to 5 cm length of either sapwood, outer heartwood or inner heartwood were transferred into a 65 mL glass vial closed with a cap and septum. All vials were flushed for 5 min at a flow rate of 0.5 L min^{-1} with an incubation mixture containing the substrates used in the hydrogenotrophic pathway (10% CO_2 and 1% H_2 in N_2). Soon after flushing, 0.2 mL of the gas inside the vials was drawn from the vial through the septum into a syringe and injected into the analyser as explained above. Other similar gas samples were collected 4, 8 and 24h after the flushing. Molar fraction in the vials at each sampling time was then calculated using equation [1]. Given that the samples were collected several hours before incubation and the incubation vials were flushed for 5 minutes, we assumed that the majority of the CH_4 initially trapped within the wood core segments (6 mm in radius) would have been released at the end of the flushing process, and that the CH_4 accumulating in the vial during incubation originated from de novo CH_4 production. The *ex-situ* methane production rate of wood was determined by calculating the maximal difference in CH_4 quantity within the vials between two sampling points, then dividing it by the duration of incubation and the dry mass of the wood core segment (Epron et al. 2023). We used the maximum concentration difference between any two time points—rather than a simple

calculation based on the start and end points—to capture potential production capacity when the concentration increase was not perfectly linear. Such a situation can arise due to concentration measurement precision, an initial activation phase following sample storage, the time required to re-establish equilibrium between production within the wood segment and diffusion at its surface, or the depletion of substrates potentially utilized by pathways other than the hydrogenotrophic pathway.

Wood physical characteristics

Before the incubation period, the fresh weight (FW), length and diameter of each wood segment was measured and its volume (V) calculated. After the incubation, each segment was stored in a freezer at 20°C, freeze-dried for at least 48 h in a freeze dryer (FDU-1200; EYELA, Tokyo, Japan), and the dry weight (DW) measured. Moisture content (MC) and bulk density (BD) were then calculated as:

$$\mathrm{MC} = \frac{\mathrm{FW} - \mathrm{DW}}{\mathrm{DW}} \quad [2]$$

$$\mathrm{BD} = \frac{\mathrm{DW}}{\mathrm{V}} \quad [3]$$

Air-filled porosity was calculated from BD and MC as:

$$\mathrm{AFP} = \Phi - \mathrm{MC} \times \mathrm{BD} \quad [4]$$

were Φ is the total porosity, calculated as:

$$\Phi = 1 - \frac{\mathrm{BD}}{\mathrm{MD}} \quad [5]$$

with MD the density of the pure cell wall material considered as constant, with a typical value of 1.51 g cm^{-3} (Kellogg & Wangaard, 1969).

Wood chemical characteristics

The freeze-dried samples were ground using a ball mill (MM-400; Retsch, Düsseldorf, Germany) for 3 min intermittently to avoid overheating.

Wood pH was measured according to Yip et al. (2018): 40mg of wood powder was mixed with 1.2 ml of ultra-pure water. After 1h incubation on a block bath shaker at room temperature,

the pH of the supernatant was measured using a LAQUAtwin pHmeter (Horiba) after centrifugation.

To extract soluble sugars and amino acids, ninety milligrams of dry wood powder was mixed with 0.75 mL of hot water at 85°C and vortexed thoroughly. An additional 0.75 mL of hot water was then added, and the mixture was incubated at 85°C for 30 minutes (adapted from Lehmann et al., 2016). After incubation, the samples were centrifuged, and the supernatant was filtered using a 0.45 µm filter. The soluble sugar concentration was determined by mixing 0.25 mL of the hot water extract with 0.5 mL of a 2% phenol solution and 1.25 mL of 95% H_2SO_4 (adapted from DuBois et al., 1956). The mixture was incubated in the dark at room temperature for 10 minutes and then cooled for 15 minutes. Absorbance was measured at 485 nm, with glucose solution (1 mg mL^{-1}) used for calibration. Amino acid concentration was determined by mixing 0.1 mL of the hot water extract with 0.3 mL of 0.4 M citrate buffer at pH 5.25 and 0.3 mL of ninhydrin. The mixture was heated at 100°C, followed by the addition of 0.75 mL of 60% ethanol before measuring the absorbance at 570 nm. Leucine solution at a concentration of 3.3 mg mL^{-1} was used for calibration. Additionally, the osmolality of the hot water extract was measured using a vapour pressure osmometer (VAPRO model 5600, ELITechGroup).

To extract phenolic compounds, twenty-five milligrams of dry wood powder was mixed with 2 mL of 99.5% ethanol and incubated at 80°C for one hour, with manual shaking every 10 minutes (Quentin et al. 2015). The supernatant was collected and stored at 4°C. This process was repeated twice with 1.5 mL of ethanol. Finally, the supernatant was filtered using a 0.45 µm filter. Phenol concentration was determined by mixing 0.05 mL of the ethanol extract with 0.25 mL of a 10-fold diluted Folin-Ciocalteu reagent in a 2 mL cuvette (adapted from Singleton & Rossi, 1965). After a 2-minute reaction time, 1 mL of 20% Na_2CO_3 was added to facilitate the oxidation-reduction process. The mixture was then incubated for 30 minutes before measuring the absorbance at 760 nm. Calibration was conducted using a gallic acid standard solution (0.5 mg mL^{-1}).

DNA extraction and bacterial community analysis

DNA was extracted from 40 mg of the ground wood powder obtained from all samples used for the incubation experiment with the FastDNA SPIN Kit for soil (MP Biomedicals, Santa Ana,

CA, USA) following the manufacturer's instructions including homogenization in a FastPrep instrument at a speed setting of 6.0 for 40 seconds. The DNA samples were further purified with a OneStep PCR Inhibitor Removal Kit (Zymo Research, Irvine, CA, USA) before PCR amplification. DNA extraction was performed in duplicate, and the reported values are the average of the duplicate samples.

Amplicon sequencing analysis targeting the V3-V4 region of bacterial 16S rRNA genes was carried out on the Illumina NextSeq 1000 (Illumina, San Diego, USA) with NextSeq 1000/2000 P1 Reagents (600 Cycles) kit as described in Harada et al. (2024). The 1st round PCR was carried out with a primer set Bakt_341F and Bakt_805R (Herlemann et al. 2011) and TaKaRa Ex Taq polymerase (TaKaRa, Kusatsu, Japan). The program consisted of the first denaturation step at 94 °C for 2 min, 35 cycles of denaturation at 94 °C for 30 s, annealing at 55 °C for 30 s, and elongation at 72 °C for 30 s, followed by the final elongation at 72 °C for 5 min. The 2nd round PCR amplification, library construction, and sequencing reaction were outsourced to the Bioengineering Lab (Sagamihara, Japan). The obtained FASTQ data were processed with Qiime2 (ver. 2021.11; Bolyen et al., 2019): removal of the primer region by the cutadapt (Martin 2011), filtering, denoising, merging of forward and reverse reads, and removing of chimera sequences with DADA2 (Callahan et al. 2016). The obtained representative amplicon sequence variants (ASVs) were classified with a trained classifier based on a data set of the EzBioCloud 16S rRNA database (Yoon et al. 2017) and mitochondrial and chloroplast sequences retrieved from Silva 138 SSURef NR99 full-length sequences (Quast et al. 2012). Then, the ASVs assigned to archaea, mitochondria and chloroplast were filtered out from the samples, followed by the calculation of the relative abundance of each taxon. The final frequency in the samples was 422–23,241 with a median of 11,844. Taxonomic names were manually revised as appropriate in accordance with the latest prokaryotic nomenclature.

In addition, real-time PCR analysis of the *mcrA* genes was performed via the Thermal Cycler Dice Real Time Sytrunk (TaKaRa, Kusatsu, Japan) and primers MLf/MLr (Luton et al. 2002), as described in Watanabe et al. (2010). Each 25-µl mixture contained TB Green Premix Ex Taq (TaKaRa), MLf/MLr primers (0.2 µmol l^{-1} each), 0.25 µl of bovine serum albumin (0.2 g l^{-1}), 2 µl of template DNA, and sterilized ultrapure water. The PCR thermal cycle was as follows: 95°C for 10 s (denaturization); 45 cycles of 95°C for 40 s (denaturization), 55°C for 30 s (annealing), and 72°C for 60 s (elongation). An increase in the PCR product was detected by the fluorescent

signal, and its threshold cycles (Ct values) were determined via the second derivative maximum method. The amplification of nonspecific DNA fragments was checked via dissociation curve analysis. The copy number of the *mcrA* gene was calculated via a standard curve generated from a series of dilutions (1.14×10^8 to 1.14×10^1 copies μl^{-1}) of the standard sample.

Amplicon sequencing analysis targeting the fungal internal transcribed spacer 1 (ITS1) region of the nuclear ribosomal DNA, was carried out as described in Matsuoka et al (2019, 2021). A two-step PCR was employed. The first-round PCR was carried out with using the ITS1-FKYO2 and ITS2-KYO2 primer sets (Toju et al. 2012). For the first PCR, the EX Taq Hot Start Version (Takara Bio, Kusatsu, Japan) was used. 0.5 µl of DNA extract, 0.1 µl of EX Taq, 1.0 µl of EX Taq Buffer, 0.8 µl (2.5 mM) of dNTP mix, 0.5 µl (10 µM) of forward and reverse primers, and 6.6 µl of nuclease-free water were used. The first PCR reaction was followed by 4 min at 94 °C, denaturation at 94 °C for 30 s, annealing at 50 °C for 30 s, and extension at 72 °C for 1 min, followed by 30 cycles of 3 steps of denaturation at 94 °C for 30 s, annealing at 50 °C for 30 s, and extension at 72 °C for 1 min, with a final extension time of 72 °C for 10 min. Illumina flow cell adapters and 8-bp identifier indices were added in the second PCR step. The second PCR was carried out with 12 µl reaction volume containing 1.0 µl of template, 6 µl of 2× KAPA HiFi HotStart ReadyMix (KAPA Biosytrunks, Wilmington, Washington, USA), 1.4 µl of each primer (2.5 µM), and 2.2 µl of sterilized distilled water. The PCR conditions were as follows; an initial incubation for 3 min at 95°C followed by 12 cycles of 20 s at 98°C, 15 s at 72°C for annealing and extension, and a final extension of 5 min at 72°C. The purified amplicon libraries were sequenced using the MiSeq v2 Reagent Kit (Illumina, San Diego, CA, USA). The resulting PCR amplicons were pooled and purified using AMPure XP (Beckman Coulter, Brea, CA, United States). The purified library was then excised using E-Gel SizeSelect (Thermo Fisher Scientific, Waltham, MA, United States). The resulting library was subjected to 2×300-bp paired-end sequencing on the MiSeq platform (Illumina, San Diego, CA, United States).

The raw MiSeq data were converted into FASTQ files using Bcl2gastq v2.18.0.12. Then the reads were processed with Claident pipeline v0.9.2022.04.28 (Tanabe and Toju 2013). First, reads were de-multiplexed using the “clsplitseq” command. After de-multiplexing, the forward and reverse reads were merged using the “clconcatpairv” command and low-quality reads were trimmed using the “clfilterseqv” command. Then potentially noisy and chimeric

sequences were eliminated using DADA2 (Callahan et al. 2016) and UCHIME (Edgar et al. 2011), respectively. In chimera removal, UNITE database was used as a reference. After this procedure, obtained reads were clustered into operational taxonomic units (OTUs) with similarity thresholds of 0.97 using the "clclassseqv" command. For each of the obtained OTUs, taxonomic identification was conducted based on the query-centric auto-k-nearest neighbour method (Tanabe and Toju 2013) with the NCBI database, and subsequent taxonomic assignment was conducted using the lowest common ancestor algorithm (Huson et al., 2007) using Claident. The functional guild of each fungal OTU was estimated based on the FungalTraits (Põlme et al. 2020). 76 OTUs were detected, including six that were not identified as fungal organisms and were therefore discarded.

Data analysis

All statistical analyses were performed in R (R Core Team 2021). Comparisons of potential production rates against zero and *in-situ* CH_4 molar fractions against atmospheric or soil CH_4 molar fractions were assessed using Wilcoxon tests. Differences in *ex-situ* CH_4 production rates and *in-situ* CH_4 molar fractions between species as well as among segments were evaluated using the aligned rank transformation test (ART), with tree ID included as a nested variable. The relationship between *ex-situ* potential CH_4 production rates and *in-situ* CH_4 molar fractions was assessed using Spearman the correlation test, applied both across the full dataset and separately for each species. A principal component analysis (PCA), performed using the FactoMineR package, were conducted across both species and all segments and included chemical variables (concentrations of soluble sugars, amino acids and phenolic compounds, as well as pH and in-situ CO_2 molar fractions), alongside physical variables (moisture content, bulk density, and air-filled porosity). Hierarchical clustering was then performed independently for each species, restricted to inner heartwood segments using the same variables, as well as the MC, BD, and AFP values of the preceding segment (outer heartwood).

Bacterial community composition was assessed using weighted UniFrac distances, which were also calculated independently for each species by considering only the inner heartwood. Data regarding the other wood core segments are available in the data repository. For clarity, only bacterial families with a relative abundance above 0.5% and a significant contribution (tested using the vegan package) were retained for visualisation. Functional predictions were carried

out using the FAPROTAX database. The congruence between hierarchical clustering based on physicochemical variables and bacterial community clustering was assessed using a Procrustes test.

Results

Potential CH_4 production and internal molar fraction of CH_4

Ex-situ potential CH_4 production and *in-situ* CH_4 molar fraction were well correlated (Fig.1a, ρ = 0.54, p = 0.02, for *F. crenata* and ρ = 0.69, p < 0.001, for *C. japonica*), indicating both variables can be used as a proxy of *in-situ* methanogenic activity. Both species showed similar *ex-situ* potential CH_4 production ranges with median values of 0.07 nmol CH_4 g^{-1} h^{-1} (range: 0.007–19.4) for *F. crenata* and 0.44 nmol g^{-1} h^{-1} (0.0007–26.2) for *C. japonica* (Fig.1b, p = 0.26). The *in-situ* CH_4 molar fractions exceeded atmospheric levels by one to five orders of magnitude in all trees with no difference between species: medians of 63 ppm (range: 25–4.6×10^5) for *F. crenata* and 62 ppm (12–4.6×10^5) for *C. japonica* (Fig.1c, p = 0.61). For both species, compared to the sapwood, the inner heartwood showed a greater *ex-situ* production (Fig.1b, ART, *Fc*: p = 0.002, *Cj*: p = 0.004) and a higher *in-situ* CH_4 molar fraction (Fig.1c, ART, *Fc*: p = 0.007, *Cj*: p = 0.005), with a stronger inter-individual variability between segments of the inner heartwood. Soil CH_4 molar fraction was lower than the ambient molar fraction at a depth of 10 cm (1.35 and 1.51 ppm in *C. japonica* and *F. crenata sites*, respectively). At the *F. crenata* site, the molar fraction increased with depth (2.18 ± 0.41 ppm at 40 cm, N=3). At the *C. japonica* site, the CH_4 molar fraction reached a peak of 2.01 ± 0.10 ppm at 20 cm depth compared to 1.95 ± 0.29 ppm at 40 cm (N=3).

Within trunk micro-environment

The first PCA axis (Fig.2a, 45% of the total variance) correlated with chemical compounds (phenols: 0.87, amino acids: -0.75, pH: 0.68, CO_2: 0.36, soluble sugars: -0.74, p < 0.001) and moisture content (MC: 0.75, p < 0.001). The second axis (20% of the total variance) was driven by bulk density and air-filled porosity (BD: 0.47, AFP: -0.88, p < 0.001) and CO_2 (0.68). Species differed significantly (Fig.2b; p < 0.001). *F. crenata* was characterized by a higher bulk density than *C. japonica*, as well as greater concentrations of soluble sugars and amino acids, whereas *C. japonica* showed higher moisture content (> 1 $g.g^{-1}$ for all samples), concentrations of phenolic compounds, and pH than *F. crenata* (Fig.S1). Furthermore, within species, the sapwood segment was different from the two other heartwood segments with concentrations of soluble sugar and amino acid 1.5–3 times higher and concentrations of phenolic compounds

5–10 times lower. The sapwood exhibited higher bulk density and lower moisture content than the heartwood (Fig.2b, Fig.S1). In addition, CO_2 molar fractions were more homogeneous in F. crenata than in C. japonica, whose sapwood showed more variable concentrations, although these did not differ significantly from those at other depths. Given their higher *in-situ* CH_4 molar fraction and *ex-situ* CH_4 production, the subsequent analyses focus on the inner heartwood segments.

Relationship between methanogenic activity and the physicochemical environment of heartwood

The hierarchical clustering grouped samples of inner heartwood of *F. crenata* according to their level of *in-situ* CH_4 molar fraction and pointed out 3 groups of individuals and three groups of variables (Fig.3). Among the individuals, Fc#1i, which exhibited the higher *in-situ* CH_4 molar fraction (4.6×10^5 ppm), had less similarities with the other samples mainly because of higher moisture content, pH and phenols and lower bulk density. The standardized variable scores (z-scores) revealed contrasting patterns across the three clusters. Fc#1i showed strongly positive scores for several variables including moisture content, pH and phenols concentration (up to +2.02, moisture content > 1 g g^{-1}), with strongly negative scores for bulk density (−1.55) and air-filled porosity (-1.18). The Fc#2i sample was different due to higher air-filled porosity and the outer heartwood segment largely wetter than the average (z-scores of +1.75 for BD and +1.25 for pre-MC). This individual exhibited the second highest *in-situ* CH_4 molar fraction (4.6×10^4 ppm). Finally, samples 3i to 6i, from individuals with the lowest *in-situ* CH_4 molar fraction, were clustered together. This largest cluster displayed generally moderate z-scores with more variable patterns, including some strongly negative values scattered across individual samples, suggesting greater within-group heterogeneity despite their overall similarity in *in-situ* CH_4 molar fraction (25 - 100 ppm).

For *C. japonica*, the hierarchical clustering revealed 3 groups. Contrary to *F. crenata*, the clustering did not group samples according to their level of *in-situ* CH_4 molar fraction (Fig.4). Sample Cj#3i, for which internal degradation was observed on wood cores (Table S1), clearly stood out from the other samples, and exhibited the lowest *in-situ* CH_4 molar fraction (12 ppm). It was characterized by strongly positive z-scores for soluble sugar and amino acid concentration (+1.8 and +2.29), while displaying strongly negative scores for preBD, preMC

and BD (−1.65, −1.47, −0.91). The second cluster grouped Cj#1i, Cj#5i and Cj#7i, showing generally negative z-scores for MC and preAFP, but more positive z-scores for AFP, preMC and preBD, particularly for Cj#1i (+1.44, +1.13, +1.77). The third cluster, comprising Cj#6i, Cj#2i, Cj#8i and Cj#4i, showed the most heterogeneous profiles, with Cj#6i exhibiting notably high MC and CO_2 molar fraction (+1.61, +1.89). Cj#2i, with the highest *in-situ* CH_4 molar fraction (2.2×10^5 ppm), exhibited the lowest *in-situ* CO_2 molar fraction and was the more acidic segment (-1.32, -1.31).

Methanogens detection

Methanogenic archaea were detected in only six samples and showed no correlation with either *in-situ* CH_4 molar fraction or *ex-situ* methanogenesis (Fig.S2). Among these, samples Fc#1i, Cj#1i, Cj#2i, and Cj#3i, which exhibited measurable methanogenic activity, harboured methanogenic archaea with gene copy numbers ranging from 10^4 to 10^7 (Fig.S2). Nonetheless, methanogens were also detected in samples with low methanogenic activity, such as Fc#3i and Fc#5i, with gene copy numbers of 10^4 (Fig.S2). Conversely, sample Fc#2i, which displayed high methanogenic activity, harboured no detectable methanogenic archaea (Fig.3).

Bacterial community

Beta diversity in the inner heartwood (UniFrac PCoA) revealed sample clustering by bacterial families taking into account bacterial families with a relative abundance above 0.5% ($p < 0.05$). For *F. crenata*, the sample Fc#5i was excluded (too low sequencing depth). The relative abundance of Bacillota was above 30% either in inner heartwood samples with the highest internal CH_4 molar fractions (Fig.5a, Fc#1i and 2i), or in the sample with the lowest CH_4 molar fraction (Fig.5a, Fc#4i). However, this particular sample had a low number of reads, which may have led to the under-detection of other families and, consequently, an overestimation of the relative abundance of Bacillota. Along PCoA Axis 1, Fc#2i and Fc#4i clustered together despite contrasting CH_4 molar fractions (15,528 vs. 87 ppm), both enriched in *Sporolactobacillaceae* (Fig.5b, Fig.6a). The samples Fc#3i and Fc#6i, grouped on axis 1 with negative coordinates, harboured mainly bacteria from Pseudomonadota phylum. Axis 2 discriminated Fc#1i, associated with *Cellulomonadaceae*, *Anaerolineaceae*, *Lachnospiraceae*, and *Oscillospiraceae* (Fig.6a). Metabolic inference analyses (FAPROTAX, Fig.S3a) showed fermentation dominated

in Fc#1i, Fc#2i and Fc#4i (Fig.S3a). Other samples were dominated by aerobic chemoheterotrophy. Nitrogen cycling functions were exclusive to Fc#3i and Fc#6i, except marginal nitrate reduction in Fc#2i. *Sporomusa malonica* (Bacillota), capable of methylotrophy and methanol oxidation appeared in samples Fc#1i and Fc#4i.

For *C. japonica*, inner heartwood samples were differentiated along axis 1 by their internal CH_4 molar fraction (Fig.6b). Samples with high [CH_4] (>100 ppm, negative coordinates on axis 1) showed a relative abundance of Bacillota in their inner heartwood above 50% (Fig.5a) in which *Sporomusaceae* and *Oscillospiraceae* were the most abundant (Fig.5b, Fig.6b), with Cj#2i having the highest relative abundance of *Oscillospiraceae*. Samples with low [CH_4] (<100 ppm, positive coordinates on axis 1) exhibited a high relative abundance of Pseudpmonadota (e.g. *Enterobacteriaceae*, *Sphingomonadaceae*) and a low relative abundance of Bacillota (Fig.5a). Within these samples, two sub-clusters emerged: positive coordinates on axis 2 (upper-right, Fig.6b, Cj#7i, Cj#8i) driven by *Enterobacteriaceae* and *Moraxellaceae*; lower-right (Cj#3i) by *Nitrobacteraceae* and *Cellulomonadaceae* from the phylum of *Actinomycetota* that represent more than 30% of the relative abundance and, from the phylum of Pseudomonadota. Metabolic inference analyses (FAPROTAX) highlighted aerobic chemoheterotrophy as the dominant source of energy (21.4-34.0%, Fig.S3b). Fermentation peaked in Cj#2i (34.3%) and Cj#3i (29.2%). Nitrogen respiration and nitrate reduction were consistent at 7-10% in Cj#4i-Cj#8i. Sample Cj#3i was the only one to harbour bacteria capable of fixing nitrogen. Genus that includes methanotrophs, were detected in Cj#3i (*Methylocapsa*, Beijerinckiaceae), and Cj#5i (*Methylobacterium*, Methylobacteriaceae), albeit at very low relative abundances. Aromatic compound degradation was the main function linked to the carbon-cycle ranging from 0.19 to 14.38%. The Procrustes analysis revealed no significant congruence between the physicochemical environment and the bacterial community composition for either *F. crenata* or *C. japonica* (Fig.7, Fc: $p = 0.29$, Cj: $p = 0.68$).

Fungal community

Among the 70 OTUs identified as fungi, only 46 of them were assigned to a fungal phylum and 27 to a family (Table S2). Among them, 19 OTUs were wood saprotrophs and 11 identified as white rot fungi. Fungal ITS1 PCR amplification was observed only in samples Cj#2o (9 OTUs), Cj#7i (6 OTUs), and Cj#8i (5 OTUs). Therefore, the fungi did not colonize the majority of the *C.*

453 *japonica* samples, making comparison of fungal communities between trees impossible. In
454 contrast, the fungal ITS1 was amplified in all inner heartwood samples of *F. crenata* except
455 Fc#3i, but the number of OTU detected was very low in Fc#1i, Fc#2i, and Fc#4i, which also
456 hinders the comparison of fungal communities between trees.

457

Discussion

Anoxic and alkaline heartwoods are the main production site of CH_4 in tree trunks

The primary objective of this study was to localise the hotspot of production in living trees. For the first time, the molar fraction was measured at different depths in the trunk of living trees and, in agreement with our first hypothesis, the internal CH_4 molar fraction was higher in the inner heartwood than in the sapwood, with values reaching up to 4.6×10^5 ppm (46 %). These values are consistent with previous measurements conducted at the same site (Mochidome and Epron 2024; Mochidome et al. 2025; Epron and Mochidome 2026) and align with observations from other forest ecosytrunks and tree species (Covey et al. 2012; Wang et al. 2017; Gewirtzman et al. 2025). Although no method currently exists to quantify actual *in situ* methanogenesis rates under natural conditions, the high CH_4 molar fraction in the heartwood, associated with high rates of *ex-situ* CH_4 production, strongly suggests that methanogenesis is the primary driver of CH_4 accumulation in the trunks of these two species in a cold-temperate upland forest. This is corroborated by the confirmed presence of methanogenic archaea in the trunks as several individuals of these two species at the same study site obtained by PCR amplification of the *mcrA* gene (Harada et al. 2024; Mochidome et al. 2025), and their greater abundance in heartwood than in sapwood (Feng et al. 2022; Gewirtzman et al. 2025; Arnold et al. 2025). Although quantifying the abundance of methanogenic archaea was not the focus of this study, the results of our qPCR analysis confirm their presence. However, the copy number of the *mcrA* gene was below the detection threshold (10^4 copies when 100 µL of DNA was extracted from a 40 mg sample) for some samples, some of which nevertheless exhibited a high potential for *ex-situ* CH_4 production (e.g., Fc#2). This result is not surprising, as the number of *mcrA* gene copies has been shown to be uncorrelated with methanogenic activity (Gewirtzman et al., 2025; Mochidome et al., 2025). Factors other than the number of methanogenic archaea, such as substrate availability, pH, and redox potential, may have contributed to the high methanogenic activity in these samples (Moisan et al. 2024).

Although the concentration of fermentable substrates (soluble sugars, amino acids) is lower in the heartwood compared to the sapwood and bark, the central part of the trunk more readily promotes anoxic conditions (Covey et al. 2012; Wang et al. 2021; Epron et al. 2023; Harada et al. 2024). O_2 diffusion is limited in wet heartwood, characterised by a high moisture

content, which can generate anoxic conditions, an environment essential for obligate anaerobes such as methanogenic archaea and therefore for biotic CH_4 production (Zeikus and Henning 1975; Wang et al. 2017; Feng et al. 2022; Epron et al. 2023). However, only one of the two species, *C. japonica*, is known to have wet heartwood (Nakada et al. 1999), and yet *ex-situ* CH_4 production and *in-situ* CH_4 accumulation did not differ significantly between the two species, and CH_4 production was highly variable in *C. japonica* heartwood. This suggests that the presence of wetwood alone is not enough to explain CH_4 production, thereby confirming the first hypothesis. Dense wood and/or preceding wood tissues with low permeability are also likely to promote the development of anoxic conditions in the inner heartwood. In line with this first hypothesis, the presence of wet heartwood was therefore not sufficient on its own to allow methanogenesis, as a strong variability was observed for this segment, highlighting the need to investigate the local physicochemical microenvironment within the heartwood to better understand methane production dynamics.

pH was more variable in *F. crenata*, which generally displayed more acidic conditions, while *C. japonica* heartwood tended toward more alkaline values. This alkalinisation is characteristic of wetwood and has been associated with the accumulation of alkaline cations, particularly potassium (Murdoch et al. 1987; Kubo and Ataka 1998; Moya et al. 2009; Okada et al. 2011, 2012). pH is a well-known regulator of methanogenesis with an optimum in neutral to slightly alkaline conditions (pH 6.5–8.0), with activity sharply declining under acidic conditions (Le Mer and Roger 2001; Conrad 2007; Ye et al. 2012; Moisan et al. 2025). This could partly explain the higher *in-situ* methanogenesis observed in Fc#1i compared to the more acidic *F. crenata* samples. Beyond its direct effect on methanogens, more acidic pH (5 – 6.5) could increase methanotrophic activity (Le Mer and Roger 2001; Moisan et al. 2025), although it was detected at very low relative abundance in only two Cj samples. Furthermore, pH also structures broader microbial communities, influencing the availability of fermentation substrates and the activity of syntrophic bacteria that supply hydrogen and acetate to methanogens (Schulz and Conrad 1996).

Soluble sugar and amino acid concentration showed a non-negligible range of variation, broadly similar between the two species, with the notable exception of Cj#3i, which displayed markedly elevated concentrations consistent with its highly degraded state. Interestingly, while Cj#3i exhibited very high *ex-situ* CH_4 production rates, the *in-situ* CH_4 molar fraction

remained moderate. This discrepancy could reflect partial escape of methane through the heartwood cavity in the central part of the trunk rather than accumulation in the tissue, or alternatively, an overestimation of the *ex-situ* production rates, as the artificial anoxic conditions imposed during the incubation experiment may not fully reflect *in-situ* conditions and provide only qualitative evidence of methanogenic capacity rather than quantitative rates (Barba et al. 2021; Epron et al. 2023).

A positive relationship between *in-situ* CH_4 and CO_2 molar fractions was expected, given that CO_2 serves as the primary substrate for hydrogenotrophic methanogenic archaea, which dominate in living trees (Feng et al. 2022; Harada et al. 2024). However, this correlation was not observed in the present study. Moreover, the ubiquitous nature of CO_2 in living trees (Teskey et al. 2008) suggests that it may not represent the limiting substrate for methanogenesis. Whether H_2 availability, as the electron donor required for hydrogenotrophic methanogenesis, represents the key limiting factor in living trees remains unknown (Leung et al. 2026). Further studies directly measuring H_2 production alongside methanogenic activity would therefore be needed to better elucidate the dynamics driving methane production within living trees.

The structure of the microbial communities evolves with the internal decay stage, in parallel with a decline in methanogenesis

The bacterial communities present in the heartwood of living trees provided complementary information on oxygen availability and gave additional evidence of the differences in methanogenic activity observed between samples. Samples with low *in-situ* CH_4 molar fraction harboured aerobic bacterial communities, including *Enterobacteriaceae* and species AJ011333 (Fc#3i, Fc#6i, Cj#7 and Cj#8, Tláskal et al., 2021). In addition, aerobic chemoheterotrophy was the dominant predicted function for those samples. In contrast, samples with higher levels of *in-situ* CH_4 molar fraction were characterised by anaerobic bacterial communities, including several families of the Bacillota phylum such as *Sporomusaceae* and *Oscillospiraceae*, which encompass facultative to obligately anaerobic species (Arnold et al. 2025). Furthermore, fermentation activity was predicted to be high in those samples, consistent with the oxygen-depleted conditions required for methanogenesis.

Beyond reflecting anoxic conditions, the microbial communities identified in high-methanogenic samples appear capable of supplying the substrates that fuel methanogenesis through the fermentative degradation of wood polymers. In the early stages of heartwood degradation, Bacillota are known to be abundant in living trees (Arnold et al. 2025), and their relative abundance increases in decomposing logs during initial wood degradation before declining as O_2 levels rise (Hoppe et al. 2015). Consistently, samples with the highest relative abundance of Bacillota were also the highest CH_4 producers, mainly visible for *C. japonica*, with *Sporomusaceae* and *Oscillospiraceae*, families encompassing obligately anaerobic species known to produce short-chain fatty acids from cellulose and hemicellulose degradation, as key discriminating taxa (Vital et al. 2014). In Fc#1i and Cj#2i, which displayed the highest CH_4 molar fractions (above 20%), additional fermentative taxa were identified: *Lachnospiraceae*, among the most important butyric acid producers (Miragoli et al. 2021; Gewirtzman et al. 2025), and *Leptolinea tardivitalis*, capable of degrading xylan and fermenting sugars (Yamada et al. 2006). In outer heartwood of Cj#2, all fungal genera recovered belonged to the wood saprotrophic guild, further supporting active decomposition. Saprotrophic fungi could also directly produced CH_4, especially species from the genus *Pleutorus*, detected in Cj#2o (Lenhart et al. 2012). It has been suggested that the energy needed for wood degradation is transported by the mycelia from oxic sites where ATP and NADH are generated by oxygenic respiration to anoxic sites where the degradation occurs (Mukhin et al 2006). Predicted fermentative activity in these samples reached approximately 30% of the relative abundance, and moisture content exceeded 1 g g^{-1}, consistent with the wet, oxygen-depleted conditions favouring both fermentation and methanogenesis. However, FAPROTAX predictions did not always capture this fermentative potential: despite CH_4 concentrations exceeding 100 ppm and the presence of anaerobic *Sporomusaceae* (e.g., *A. hongkongensis*, *S. malonica*; BacDive) in several *C. japonica* samples rich in Bacillota, fermentative activity was not prominently predicted (except for Cj#2i). This discrepancy likely reflects the limitations of functional inference tools in capturing the full metabolic potential of poorly characterised taxa, rather than an actual absence of fermentation.

As degradation progresses and heartwood hollows develop, increased wood permeability promotes oxygen transport, shifting microbial communities away from anaerobic assemblages and reducing methanogenesis (Schwarze 2007; Covey et al. 2012). In both Cj#3i

and Fc#6i, signs of advanced degradation were observed during coring and confirmed by physical and chemical analyses. Their bacterial communities reflected this shift: *Caulobacteraceae* and *Sphingomonadaceae*, involved in lignin degradation (Wilhelm et al. 2019; Gu et al. 2022), were identified in Fc#6i, while Cj#3i was characterised by taxa typical of deadwood such as *Cellulomonas* and *Bradyrhizobium* (Tláskal et al. 2017, 2021). Aerobic chemoheterotrophy was the predominant predicted function in both samples, and N-fixation was predicted for Cj#3i, a function documented in deadwood communities (Tláskal et al. 2017). Fungal communities in Fc#6i and Fc#5 were dominated by white-rot saprotrophs capable of substantial lignin degradation, further supporting ongoing decomposition. Although no clear evidence of advanced degradation was visually observed along the wood core taken from Fc#3i, the close phylogenetic proximity of its bacterial community to Fc#6i suggests that this heartwood may have already been too degraded to sustain active methanogenesis.

Microsite heterogeneity and temporal dynamics: key challenges ahead

These findings must be interpreted in light of several methodological limitations that point to important directions for future research. At the spatial scale, core segments integrate conditions across several centimetres of heartwood, yet methanogenesis and the fermentative processes sustaining it likely occur in discrete microsites where oxygen depletion, moisture, and substrate availability differ substantially from bulk conditions. Mismatches between *in-situ* CH_4 molar fraction and *ex-situ* CH_4 production, such as the high *in-situ* but low *ex-situ* production in Fc#6i, or the reversed pattern in Cj#3i, illustrate how localised production hotspots or shifting physicochemical conditions within a segment may be obscured by bulk community profiling; resolving these microsite dynamics would require spatially explicit sampling or micro-scale imaging approaches. It is also possible that the hottest spot of CH_4 production was not always sampled, given that, in this study, wood cores were collected at only a single height and in a single direction for each individual.

On a temporal scale, our synchronic approach comparing several individuals at a single point in time implicitly treats each tree as a snapshot of a shared degradation trajectory, an assumption analogous to chronosequences which cannot account for alternative trajectories driven by differences in microbial inoculum, wood chemistry, or local climate, nor for variation

in the intensity or duration of each decay stage between individuals. This could explain the lack of a significant congruence between the physicochemical environment and the bacterial community composition. It would therefore be essential to track how microbial communities, gas concentrations, and wood properties co-evolve within the same trees over time, through repeated, diachronic monitoring, to move beyond this static picture toward a dynamic understanding of methane production throughout a tree's life.

Acknowledgements

We thank the Ashiu Forest Research Station for access to the site and support. We are grateful to Makoto Nagasawa fieldwork assistance. We also appreciate discussions with Dr Shitephen Wang and Sumonta Paul. This work was supported by a grant from the Research Institute for Sustainable Humanosphere, Kyoto University and the Japan Society for the Promotion of Science (KAKENHI grant no. 24K01797), and benefited from additional funding of the exploratory research program FairCarboN from the Agence Nationale de la Recherche under the France 2030 program (ANR-22-PEXF-001). The authors would like to thank the ORION program for its contribution to the funding of NC's research internship. This work has benefited from a government grant managed by the Agence Nationale de la Recherche with the reference ANR-20-SFRI-0009

Accession number

The raw sequencing data of V3-V4 region of bacterial 16S rRNA genes and fungal ITS1 region of the nuclear ribosomal DNA were deposited in the SRA database under the BioProject accession number PRJDB42342 with DRR1051729-DRR1051760 and BioProject accession number PRJDB42462 with DRR1060532- DRR1060547, respectively.

Data availability

The data used in this study are available in The Kyoto University Research Information Repository (KURENAI, DOI: to be added after revision)

Author contributions

NC conceived the research, which was designed by NC and DE. NC, TM and DE conducted field work. NC and TM conducted DNA extraction and TW, SA and SM performed quantitative polymerase chain reaction. NC and DE analyzed data with support from TW, SA and SM for microbial communities analyzes and from MD, CP and DD for wood microenvironment analyzes. NC and DE wrote the first draft, which was then critically reviewed by all of the co-authors.

References

Arnold W, Gewirtzman J, Raymond PA, et al (2025) A diverse and distinct microbiome inside living trees. Nature 644:1039–1048. https://doi.org/10.1038/s41586-025-09316-0

Barba J, Poyatos R, Capooci M, Vargas R (2021) Spatiotemporal variability and origin of CO_2 and CH_4 tree stem fluxes in an upland forest. Glob Change Biol 27:4879–4893. https://doi.org/10.1111/gcb.15783

Bolyen E, Rideout JR, Dillon MR, et al (2019) Reproducible, interactive, scalable and extensible microbiome data science using QIIME 2. Nat Biotechnol 37:852–857. https://doi.org/10.1038/s41587-019-0209-9

Callahan BJ, McMurdie PJ, Rosen MJ, et al (2016) DADA2: High-resolution sample inference from Illumina amplicon data. Nat Methods 13:581–583. https://doi.org/10.1038/nmeth.3869

Conrad R (2007) Microbial Ecology of Methanogens and Methanotrophs. In: Advances in Agronomy. Elsevier, pp 1–63

Covey KR, Wood SA, Warren II RJ, et al (2012) Elevated methane concentrations in trees of an upland forest. Geophys Res Lett 39:. https://doi.org/10.1029/2012GL052361

Demirel B, Scherer P (2008) The roles of acetotrophic and hydrogenotrophic methanogens during anaerobic conversion of biomass to methane: A review. Rev Environ Sci Biotechnol 7:173–190. https://doi.org/10.1007/s11157-008-9131-1

DuBois M, Gilles KA, Hamilton JK, et al (1956) Colorimetric Method for Determination of Sugars and Related Substances. Anal Chem 28:350–356. https://doi.org/10.1021/ac60111a017

Epron D, Mochidome T (2026) Methane concentration in the heartwood of living trees in a cold temperate mountain forest: variation, transport and emission. Tree Physiol 46:96–107. https://doi.org/doi.org/10.1093/treephys/tpae122

Epron D, Mochidome T, Nishitsuji E, Dannoura M (2026) Are trees source or sink of methane in a cool-temperate mountain forest? Tree Physiol 46:tpaf150. https://doi.org/10.1093/treephys/tpaf150

Epron D, Mochidome T, Tanabe T, et al (2023) Variability in Stem Methane Emissions and Wood Methane Production of Different Tree Species in a Cold Temperate Mountain Forest. Ecosystems. https://doi.org/10.1007/s10021-022-00795-0

Feng H, Guo J, Ma X, et al (2022) Methane emissions may be driven by hydrogenotrophic methanogens inhabiting the stem tissues of poplar. New Phytol 233:182–193. https://doi.org/10.1111/nph.17778

Flanagan LB, Nikkel DJ, Scherloski LM, et al (2021) Multiple processes contribute to methane emission in a riparian cottonwood forest ecosystem. New Phytol 229:1970–1982. https://doi.org/10.1111/nph.16977

Gauci V, Pangala SR, Shenkin A, et al (2024) Global atmospheric methane uptake by upland tree woody surfaces. Nature 631:796–800. https://doi.org/10.1038/s41586-024-07592-w

683 Gewirtzman J, Arnold W, Taylor M, et al (2025) Tree microbiomes and methane emissions in upland
684 forests. bioRxiv

685 Gu D, Xiang X, Wu Y, et al (2022) Synergy between fungi and bacteria promotes polycyclic aromatic
686 hydrocarbon cometabolism in lignin-amended soil. J Hazard Mater 425:127958.
687 https://doi.org/10.1016/j.jhazmat.2021.127958

688 Harada M, Endo A, Wada S, et al (2024) Ubiquity of methanogenic archaea in the trunk of coniferous
689 and broadleaved tree species in a mountain forest. Antonie Van Leeuwenhoek 117:107.
690 https://doi.org/10.1007/s10482-024-02004-5

691 Herlemann DPR, Labrenz M, Jürgens K, et al (2011) Transitions in bacterial communities along the
692 2000 km salinity gradient of the Baltic Sea. ISME J 5:1571–1579.
693 https://doi.org/10.1038/ismej.2011.41

694 Hoppe B, Krüger D, Kahl T, et al (2015) A pyrosequencing insight into sprawling bacterial diversity and
695 community dynamics in decaying deadwood logs of Fagus sylvatica and Picea abies. Sci Rep
696 5:9456. https://doi.org/10.1038/srep09456

697 Jeffrey LC, Maher DT, Tait DR, et al (2020) Tree stem methane emissions from subtropical lowland
698 forest (Melaleuca quinquenervia) regulated by local and seasonal hydrology.
699 Biogeochemistry 151:273–290. https://doi.org/10.1007/s10533-020-00726-y

700 Kubo T, Ataka S (1998) Blackening of sugi (Cryptomeria japonica D. Don) heartwood in relation to
701 metal content and moisture content. J Wood Sci 44:137–141.
702 https://doi.org/10.1007/BF00526259

703 Le Mer J, Roger P (2001) Production, oxidation, emission and consumption of methane by soils: A
704 review. Eur J Soil Biol 37:25–50. https://doi.org/10.1016/S1164-5563(01)01067-6

705 Lehmann MM, Wegener F, Barthel M, et al (2016) Metabolic Fate of the Carboxyl Groups of Malate
706 and Pyruvate and their Influence on δ13C of Leaf-Respired CO2 during Light Enhanced Dark
707 Respiration. Front Plant Sci 7:. https://doi.org/10.3389/fpls.2016.00739

708 Lenhart K, Bunge M, Ratering S, et al (2012) Evidence for methane production by saprotrophic fungi.
709 Nat Commun 3:1046. https://doi.org/10.1038/ncomms2049

710 Leung PM, Jeffrey LC, Bay SK, et al (2026) Bark microbiota modulate climate-active gas fluxes in
711 Australian forests. Science 391:eadu2182. https://doi.org/10.1126/science.adu2182

712 Luton PE, Wayne JM, Sharp RJ, Riley PW (2002) The mcrA gene as an alternative to 16S rRNA in the
713 phylogenetic analysis of methanogen populations in landfill. Microbiology 148:3521–3530.
714 https://doi.org/10.1099/00221287-148-11-3521

715 Martin M (2011) Cutadapt removes adapter sequences from high-throughput sequencing reads.
716 EMBnet.journal 17:10. https://doi.org/10.14806/ej.17.1.200

717 Matsuoka S, Sugiyama Y, Sato H, et al (2019) Spatial structure of fungal DNA assemblages revealed
718 with eDNA metabarcoding in a forest river network in western Japan. Metabarcoding
719 Metagenomics 3:e36335. https://doi.org/10.3897/mbmg.3.36335

Matsuoka S, Sugiyama Y, Shimono Y, et al (2021) Evaluation of seasonal dynamics of fungal DNA assemblages in a flow-regulated stream in a restored forest using eDNA metabarcoding. Environ Microbiol 23:4797–4806. https://doi.org/10.1111/1462-2920.15669

Miragoli F, Patrone V, Prandini A, et al (2021) A mixture of quebracho and chestnut tannins drives butyrate-producing bacteria populations shift in the gut microbiota of weaned piglets. PLOS ONE 16:e0250874. https://doi.org/10.1371/journal.pone.0250874

Mochidome T, Epron D (2024) Drivers of intra-individual spatial variability in methane emissions from tree trunks in upland forest. Trees. https://doi.org/10.1007/s00468-024-02501-0

Mochidome T, Hölttä T, Asakawa S, et al (2025) Local methanogenesis drives significant methane emissions from upper tree trunks in a cool-temperate upland forest. New Phytol 247:2049–2062. https://doi.org/10.1111/nph.70331

Moisan M-A, Lajoie G, Constant P, et al (2024) How tree traits modulate tree methane fluxes: A review. Sci Total Environ 940:173730. https://doi.org/10.1016/j.scitotenv.2024.173730

Moisan M-A, Maire V, Isabelle J, et al (2025) Tissue humidity and pH as important species traits regulating tree methane emissions in floodplain wetland forests. New Phytol 248:1713–1727. https://doi.org/10.1111/nph.70543

Moya R, Muñoz F, Jeremic D, Berrocal A (2009) Visual identification, physical properties, ash composition, and water diffusion of wetwood in *Gmelina arborea*. Can J For Res 39:537–545. https://doi.org/10.1139/X08-193

Mukhin V, Voronin P (2007) Methane emission during wood fungal decomposition. Dokl Biol Sci 413:159–160. https://doi.org/10.1134/S0012496607020202

Mukhin VA, Voronin PYu, Ladatko VA, Ivanov AN (2006) The oxygenic and cooperative respiration of the wood-decaying fungus Fomitopsis pinicola (Sw.: Fr.) Pers. Dokl Biol Sci 407:153–154. https://doi.org/10.1134/S0012496606020116

Murdoch CW, Campana RJ, Biermann CJ (1987) Physical and chemical properties of wet wood in american elm *(Ulmus americana)*. Can J Plant Pathol 9:20–23. https://doi.org/10.1080/07060668709501906

Nakada R (2006) Within-Stem Water Distribution in Living Trees Of Some Conifers. IAWA J 27:313–327. https://doi.org/10.1163/22941932-90000157

Nakada R, Fujisawa Y, Hirakawa Y (1999) Soft X-ray observation of water distribution in the stem ofCryptomeria japonica D. Don II: Types found in wet-area distribution patterns in transverse sections of the stem. J Wood Sci 45:194–199. https://doi.org/10.1007/BF01177725

Nakada R, Fujisawa Y, Yamashita K, Hirakawa Y (2003) Changes in water distribution in heartwood along stem axes in Cryptomeria japonica. J Wood Sci 49:107–115. https://doi.org/10.1007/s100860300017

Okada N, Hirakawa Y, Katayama Y (2011) Application of activable tracers to investigate radial movement of minerals in the stem of Japanese cedar (Cryptomeria japonica). J Wood Sci 57:421–428. https://doi.org/10.1007/s10086-011-1188-8

Okada N, Hirakawa Y, Katayama Y (2012) Radial movement of sapwood-injected rubidium into heartwood of Japanese cedar (Cryptomeria japonica) in the growing period. J Wood Sci 58:1–8. https://doi.org/10.1007/s10086-011-1218-6

Pangala SR, Hornibrook ERC, Gowing DJ, Gauci V (2015) The contribution of trees to ecosystem methane emissions in a temperate forested wetland. Glob Change Biol 21:2642–2654. https://doi.org/10.1111/gcb.12891

Pangala SR, Moore S, Hornibrook ERC, Gauci V (2013) Trees are major conduits for methane egress from tropical forested wetlands. New Phytol 197:524–531. https://doi.org/10.1111/nph.12031

Pitz S, Chang C-H, Szlávecz K, Megonigal P (2018) Methane fluxes from tree stems and soils along a habitat gradient. Biogeochemistry 137:. https://doi.org/10.1007/s10533-017-0400-3

Plain C, Ndiaye F, Bonnaud P, et al (2019) Impact of vegetation on the methane budget of a temperate forest. New Phytol 221:1447–1456. https://doi.org/10.1111/nph.15452

Quast C, Pruesse E, Yilmaz P, et al (2012) The SILVA ribosomal RNA gene database project: improved data processing and web-based tools. Nucleic Acids Res 41:D590–D596. https://doi.org/10.1093/nar/gks1219

Quentin AG, Pinkard EA, Ryan MG, et al (2015) Non-structural carbohydrates in woody plants compared among laboratories. Tree Physiol tpv073. https://doi.org/10.1093/treephys/tpv073

R Core Team (2021) R: A language and environment for statistical computing. Published online 2021

Sakabe A, Takahashi K, Azuma W, et al (2021) Controlling Factors of Seasonal Variation of Stem Methane Emissions From Alnus japonica in a Riparian Wetland of a Temperate Forest. J Geophys Res Biogeosciences 126:e2021JG006326. https://doi.org/10.1029/2021JG006326

Saunois M, Stavert AR, Poulter B, et al (2020) The Global Methane Budget 2000–2017. Earth Syst Sci Data 12:1561–1623. https://doi.org/10.5194/essd-12-1561-2020

Schink B, Ward JC (1984) Microaerobic and Anaerobic Bacterial Activities Involved in Formation of Wetwood and Discoloured Wood. IAWA J 5:105–109. https://doi.org/10.1163/22941932-90000872

Schulz S, Conrad R (1996) Influence of temperature on pathways to methane production in the permanently cold profundal sediment of Lake Constance. FEMS Microbiol Ecol 20:1–14. https://doi.org/10.1111/j.1574-6941.1996.tb00299.x

Schwarze FWMR (2007) Wood decay under the microscope. Fungal Biol Rev 21:133–170. https://doi.org/10.1016/j.fbr.2007.09.001

Senevirathne CK, Huff A, Datta D, et al (2026) Forest health, heart rot disease, and their impact on the source of carbon-based greenhouse gas fluxes. New Phytol 250:921–933. https://doi.org/10.1111/nph.71005

Singleton VL, Rossi JA (1965) Colorimetry of Total Phenolics with Phosphomolybdic-Phosphotungstic Acid Reagents. Am J Enol Vitic 16:144–158. https://doi.org/10.5344/ajev.1965.16.3.144

796 Smits KM, Grant DS, Johnston SE, et al (2022) Riparian Cottonwood Trees and Adjacent River
797 Sediments Have Different Microbial Communities and Produce Methane With Contrasting
798 Carbon Isotope Compositions. J Geophys Res Biogeosciences 127:e2021JG006699.
799 https://doi.org/10.1029/2021JG006699

800 Tanabe AS, Toju H (2013) Two New Computational Methods for Universal DNA Barcoding: A
801 Benchmark Using Barcode Sequences of Bacteria, Archaea, Animals, Fungi, and Land Plants.
802 PLoS ONE 8:e76910. https://doi.org/10.1371/journal.pone.0076910

803 Terazawa K, Yamada K, Ohno Y, et al (2015) Spatial and temporal variability in methane emissions
804 from tree stems of Fraxinus mandshurica in a cool-temperate floodplain forest.
805 Biogeochemistry 123:349–362. https://doi.org/10.1007/s10533-015-0070-y

806 Teskey RO, Saveyn A, Steppe K, McGuire MA (2008) Origin, fate and significance of CO_2 in tree stems.
807 New Phytol 177:17–32. https://doi.org/10.1111/j.1469-8137.2007.02286.x

808 Tláskal V, Pylro VS, Žifčáková L, Baldrian P (2021) Ecological Divergence Within the Enterobacterial
809 Genus Sodalis: From Insect Symbionts to Inhabitants of Decomposing Deadwood. Front
810 Microbiol 12:668644. https://doi.org/10.3389/fmicb.2021.668644

811 Tláskal V, Zrůstová P, Vrška T, Baldrian P (2017) Bacteria associated with decomposing dead wood in
812 a natural temperate forest. FEMS Microbiol Ecol 93:. https://doi.org/10.1093/femsec/fix157

813 Toju H, Tanabe AS, Yamamoto S, Sato H (2012) High-Coverage ITS Primers for the DNA-Based
814 Identification of Ascomycetes and Basidiomycetes in Environmental Samples. PLoS ONE
815 7:e40863. https://doi.org/10.1371/journal.pone.0040863

816 Vital M, Howe AC, Tiedje JM (2014) Revealing the Bacterial Butyrate Synthesis Pathways by Analyzing
817 (Meta)genomic Data. mBio 5:e00889-14. https://doi.org/10.1128/mBio.00889-14

818 Wang Z-P, Han S-J, Li H-L, et al (2017) Methane Production Explained Largely by Water Content in the
819 Heartwood of Living Trees in Upland Forests. J Geophys Res Biogeosciences 122:2479–2489.
820 https://doi.org/10.1002/2017JG003991

821 Wang Z-P, Wu H-H, Han S-J, et al (2021) Methane Concentration in the Heartwood of Living Trees and
822 Estimated Methane Emission on Stems in Upland Forests. Ecosystems 24:1485–1499.
823 https://doi.org/10.1007/s10021-020-00596-3

824 Watanabe T, Wang G, Taki K, et al (2010) Vertical changes in bacterial and archaeal communities with
825 soil depth in Japanese paddy fields. Soil Sci Plant Nutr 56:705–715.
826 https://doi.org/10.1111/j.1747-0765.2010.00511.x

827 Welch B, Gauci V, Sayer EJ (2019) Tree stem bases are sources of CH_4 and N_2O in a tropical forest on
828 upland soil during the dry to wet season transition. Glob Change Biol 25:361–372.
829 https://doi.org/10.1111/gcb.14498

830 Wilhelm RC, Singh R, Eltis LD, Mohn WW (2019) Bacterial contributions to delignification and
831 lignocellulose degradation in forest soils with metagenomic and quantitative stable isotope
832 probing. ISME J 13:413–429. https://doi.org/10.1038/s41396-018-0279-6

833 Yamada T, Sekiguchi Y, Hanada S, et al (2006) Anaerolinea thermolimosa sp. nov., Levilinea
834 saccharolytica gen. nov., sp. nov. and Leptolinea tardivitalis gen. nov., sp. nov., novel
835 filamentous anaerobes, and description of the new classes Anaerolineae classis nov. and

836 Caldilineae classis nov. in the bacterial phylum Chloroflexi. Int J Syst Evol Microbiol 56:1331–
837 1340. https://doi.org/10.1099/ijs.0.64169-0

838 Ye R, Jin Q, Bohannan B, et al (2012) pH controls over anaerobic carbon mineralization, the efficiency
839 of methane production, and methanogenic pathways in peatlands across an ombrotrophic–
840 minerotrophic gradient. Soil Biol Biochem 54:36–47.
841 https://doi.org/10.1016/j.soilbio.2012.05.015

842 Yip DZ, Veach AM, Yang ZK, et al (2018) Methanogenic Archaea dominate mature heartwood habitats
843 of Eastern Cottonwood (Populus deltoides). New Phytol 222:115–121.
844 https://doi.org/10.1111/nph.15346

845 Yoon S-H, Ha S-M, Kwon S, et al (2017) Introducing EzBioCloud: a taxonomically united database of
846 16S rRNA gene sequences and whole-genome assemblies. Int J Syst Evol Microbiol 67:1613–
847 1617. https://doi.org/10.1099/ijsem.0.001755

848 Zeikus JG, Henning DL (1975) Methanobacterium arbophilicum sp. nov. An obligate anaerobe isolated
849 from wetwood of living trees. Antonie Van Leeuwenhoek 41:543–552.
850 https://doi.org/10.1007/BF02565096

851

852

853

Figures contents

Figure 1. Methane production and molar fractions along the radius of trunks of *Fagus crenata* (Fc) and *Cryptomeria japonica* (Cj). (a) Correlation between *ex situ* CH_4 production rates and *in-situ* CH_4 molar fractions. (b) variability in potential CH_4 production rates in wood segments quantified following a 24-hour anoxic incubation (N_2, 10% CO_2, 1% H_2) at 25°C. Wood cores from six *F. crenata* (green) and eight *C. japonica* (red) individuals were partitioned into sapwood (SW, circles), outer heartwood (oHW, triangles), and inner heartwood (iHW, squares). (c) variability in *in-situ* CH_4 molar fractions at the location of these segments. (d) variability in *in-situ* CO_2 molar fractions at the location of these segments. All numerical axes are in log scales. Solid line shows the correlation between methane production and molar fraction (Spearman correlation, $p < 0.05$). For boxplots, horizontal lines indicate medians, boxes represent the interquartile range, and individual are plotted. In addition, the level of methane production or molar fraction for each tree identified with points were linked by a dotted line. Different lowercase letters indicate significant differences between segments ($p < 0.05$) based on Aligned Rank Transform (ART) followed by post-hoc testing. Differences between species for each type of segments were not significant.

Figure 2. Principal component analysis (PCA) of physicochemical variables characterising the environment in wood segments. Biplots showing (a) variable vectors and (b) individual samples for *F. crenata* (green) and *C. japonica* (red). Explanatory variables include moisture content (MC), bulk density (BD), air-filled porosity (AFP), pH, *in-situ* CO_2 molar fraction in the trunk, and concentrations of soluble sugars (SS), amino acids (AA), and phenolic compounds. Variable arrows are coloured according to their contribution (grey scale). Symbols represent segment types: inner heartwood (iHW, square), outer heartwood (oHW, triangle), and sapwood (SW, circle).

Figure 3. Hierarchical clustering heatmap of physicochemical parameters for inner heartwood segment of *Fagus crenata*. The heatmap displays the normalized distribution (z-scores) of physicochemical variables across the six inner heartwood segments (1i–6i). Explanatory variables include moisture content (MC), bulk density (BD), air-filled porosity (AFP), pH, *in-situ* CO_2 molar fraction in the trunk (trunkCO2), and concentrations of soluble sugars (SS.concentration), amino acids (AA.concentration), and phenolic compounds

(Phenol.concentration). The MC, BD, and AFP values of the preceding segment (outer heartwood) were also included (preMC, preBD, and preAFP). The column dendrogram (top) clusters variables based on their co-variance patterns, while the row dendrogram (left) groups samples according to the similarity of their physicochemical profiles. Clusters are separated by large white cell borders. *In-situ* CH_4 molar fraction and *ex-situ* methanogenesis were excluded from the clustering analysis but are displayed as a coloured side-bar on the left to allow for a direct comparison between the observed clusters and the methanogenic gradient.

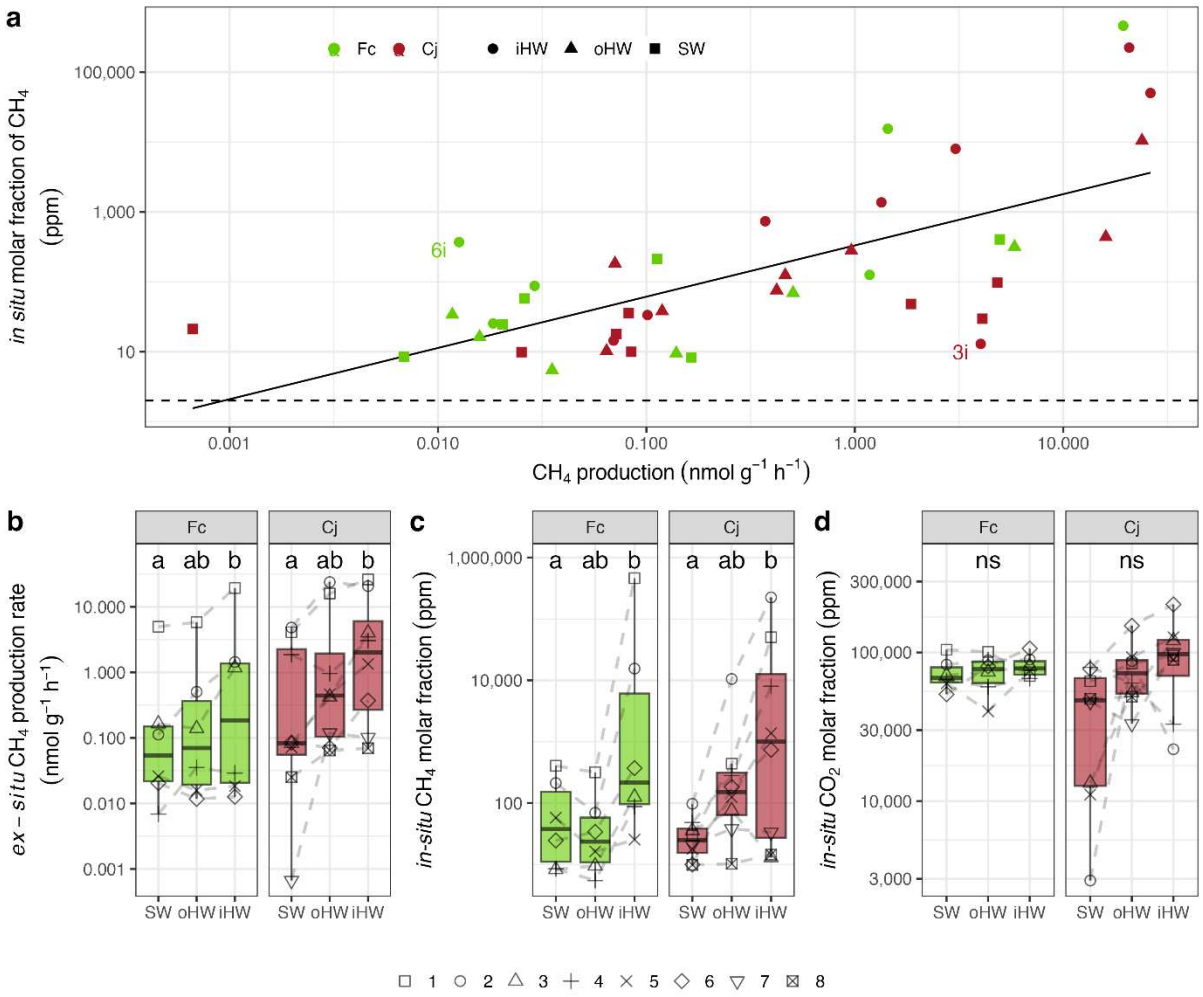
Figure 4. Hierarchical clustering heatmap of physicochemical parameters for inner heartwood segment of *Cryptomeria japonica*. The heatmap displays the normalized distribution (Z-scores) of physicochemical variables across the eight inner heartwood segments (1i–8i). Explanatory variables include moisture content (MC), bulk density (BD), air-filled porosity (AFP), pH, *in-situ* CO_2 molar fraction in the trunk (trunkCO2), and concentrations of soluble sugars (SS.concentration), amino acids (AA.concentration), and phenolic compounds (Phenol.concentration). The MC, BD, and AFP values of the preceding segment (outer heartwood) were also included (preMC, preBD, and preAFP). The column dendrogram (top) clusters variables based on their co-variance patterns, while the row dendrogram (left) groups samples according to the similarity of their physicochemical profiles. Clusters are separated by large white cell borders. *In-situ* CH_4 molar fraction and *ex-situ* methanogenesis were excluded from the clustering analysis but are displayed as a coloured side-bar on the left to allow for a direct comparison between the observed clusters and the methanogenic gradient.

Figure 5. Relative abundance of bacteria phylum (a) and Bacillota families (b) in the inner heartwood of *F. crenata* and *C. japonica*. Samples are ranked based on their *in-situ* CH_4 molar fraction from the highest (left) to the lowest (right) for each species.

Figure 6. Bacterial community structure in the inner heartwood. (a) Principal Coordinate Analysis for *F. crenata* (PCoA) based on weighted UniFrac distances of 16S rRNA gene sequences. (b) Phylogenetic tree of samples of *F. crenata*. (c) PCoA for *C. japonica*. (d) Phylogenetic tree of samples of *C. japonica*. Arrows in PCoA represent bacterial families with significant contributions ($p<0.05$) and relative abundance >0.5%, coloured by phylum. Arrow length indicates the strength of contribution; direction indicates the gradient of highest

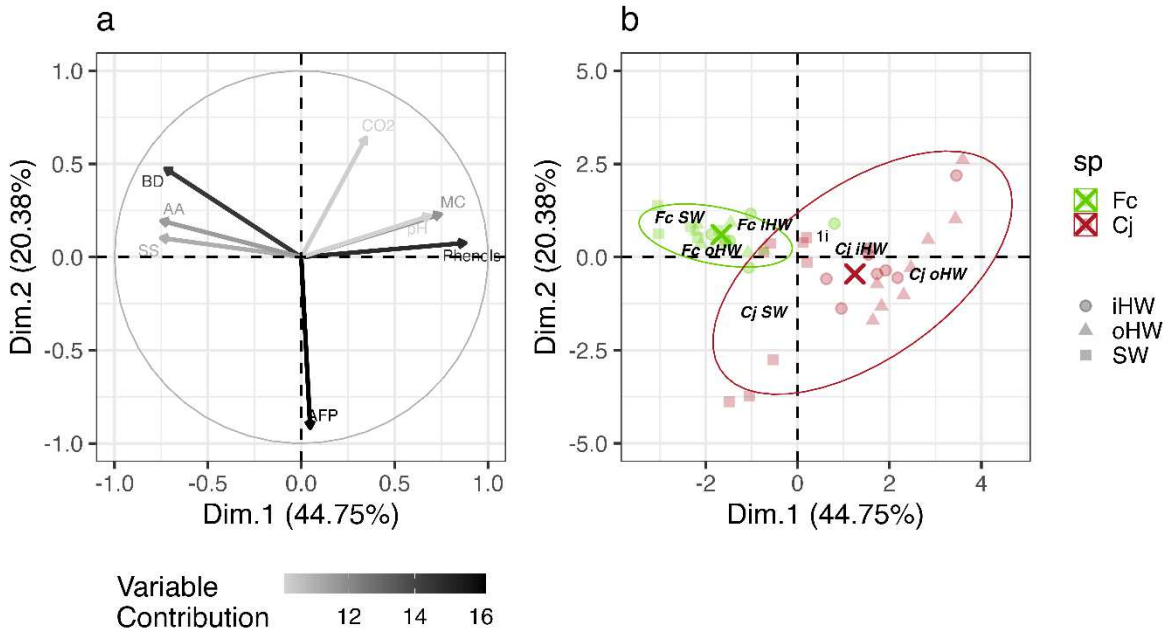
relative abundance. Samples are coloured by *in situ* CH_4 molar fraction (log-transformed ppm). *Anaerolineaceae* (Anaero.), *Bauldia* (Bauldi.), *Nitrobacteraceae* (Nitrob), *Caulobacteraceae* (Caulob.), *Cellulomonadaceae* (Cellul.), *Comamonadaceae* (Comamo.), *Desulfitobacterium* (Desulf.), *Enterobacteriaceae* (Entero.), *Erwiniaceae* (Erwini.), *Hydrogenispora* (Hydrog.), *Hyphomicrobiaceae* (Hyphom.), *Lachnospiraceae* (Lachno.), *Moraxellaceae* (Moraxe.), *Pseudomonadaceae* (Pseudo.), *Oscillospiraceae* (Oscill.), *Sphingomonadaceae* (Sphing.), *Sporolactobacillaceae* (Sporol.), *Sporomusaceae* (Sporom.), *Staphylococcaceae* (Staphy.), *Steroidobacter* (Steroi.), *Lysobacteraceae* (Lysoba.)

Figure 7. Procustres errors and ordinations comparing physicochemical parameters and bacterial community composition. Procustres rotation was performed to evaluate the congruence between ordination of the physico-chemical environment (circles) and the bacterial composition (triangles) for *Fagus crenata* (a) and *Cryptomeria japonica* (b).



927

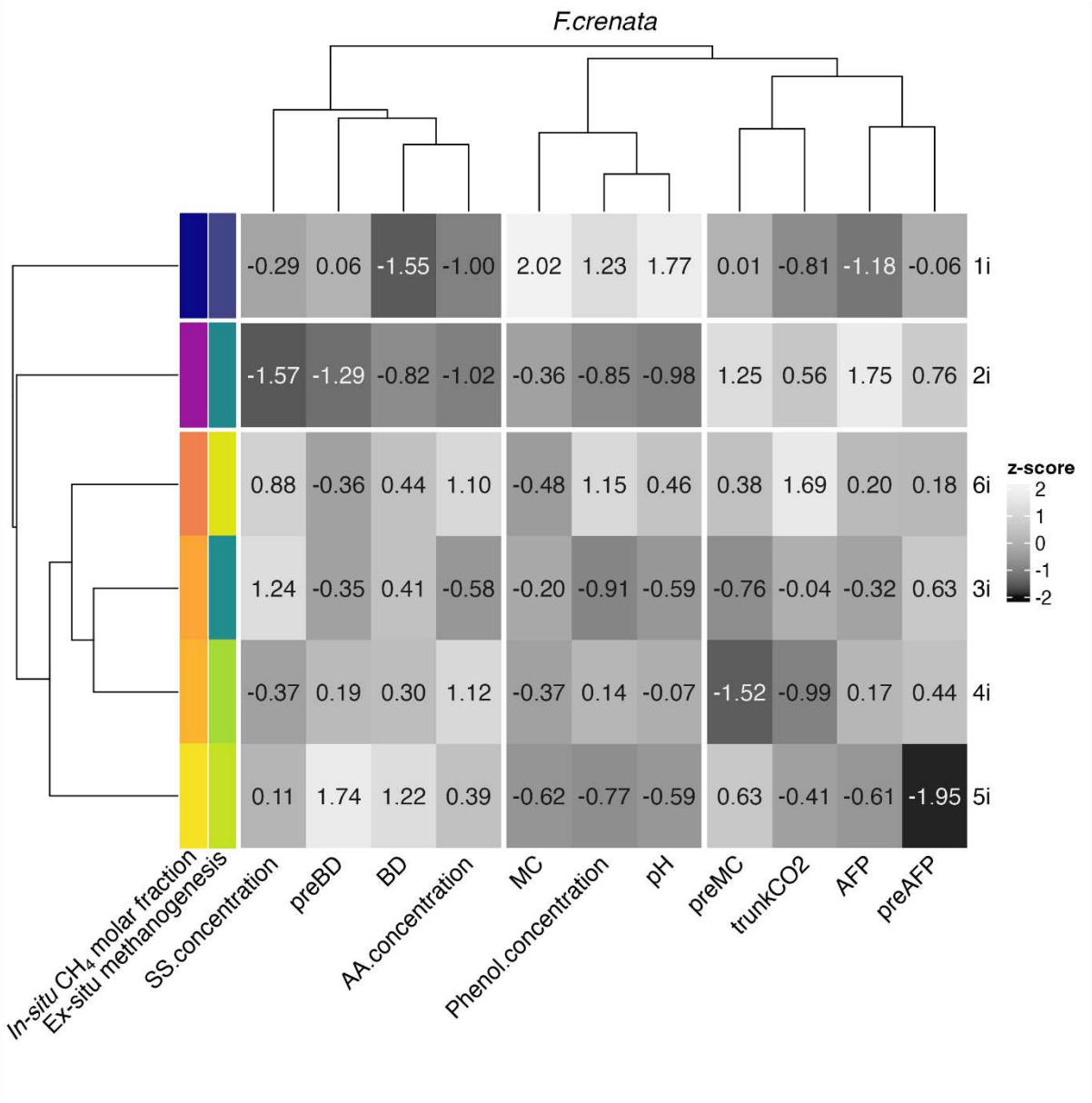
928 **Figure 1**



929

930 **Figure 2**

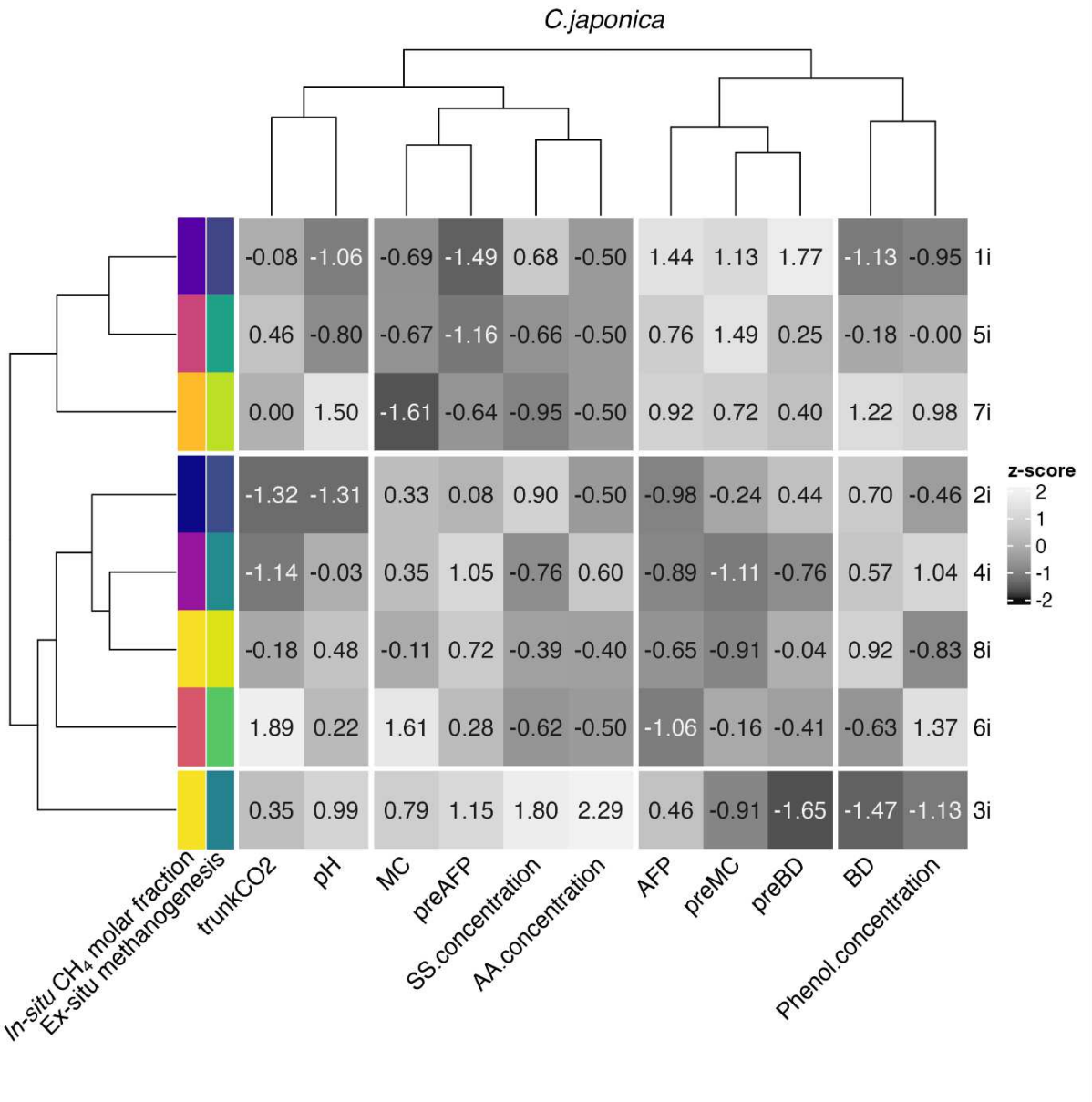
931



932

933 **Figure 3.**

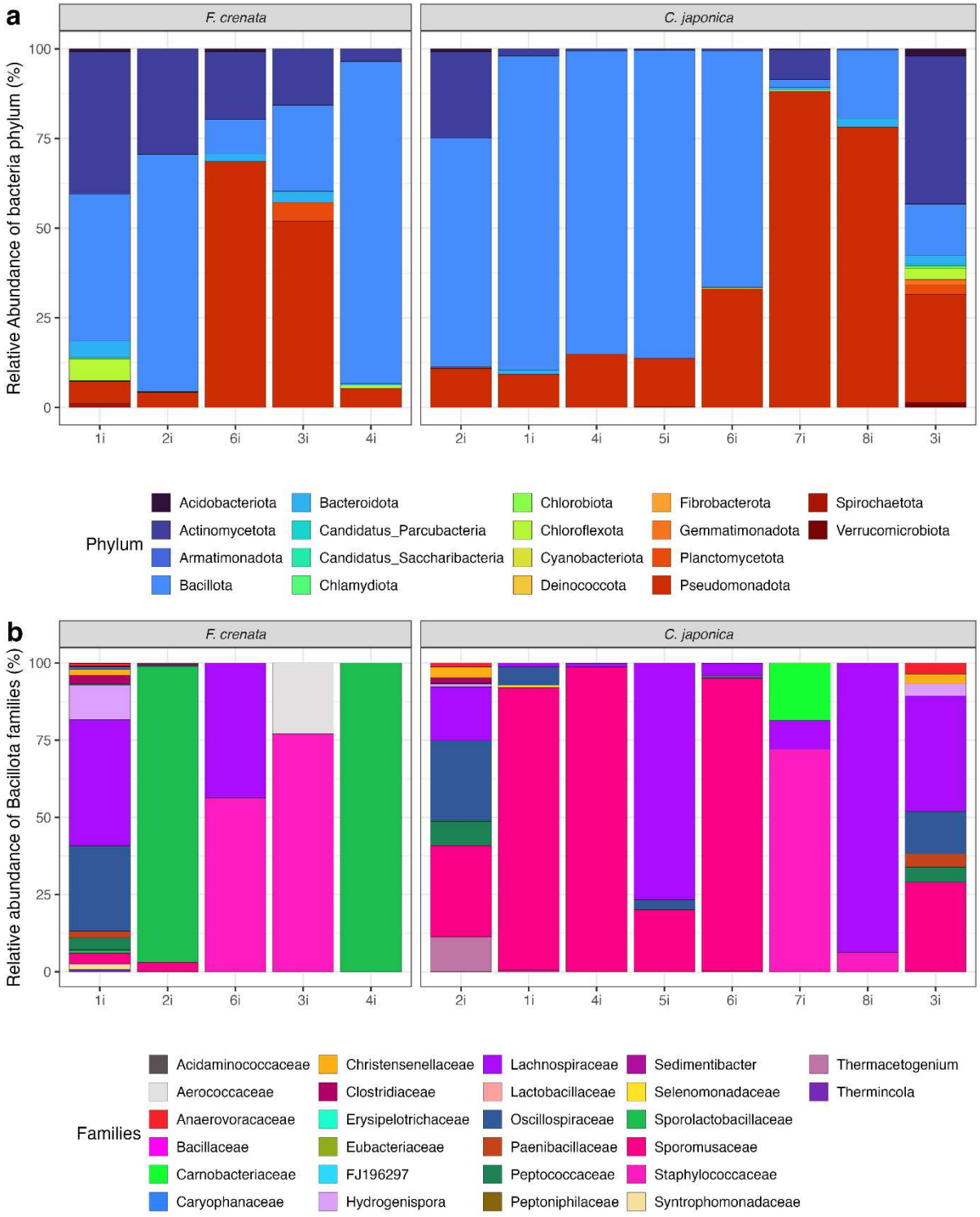
934



935

936 **Figure 4.**

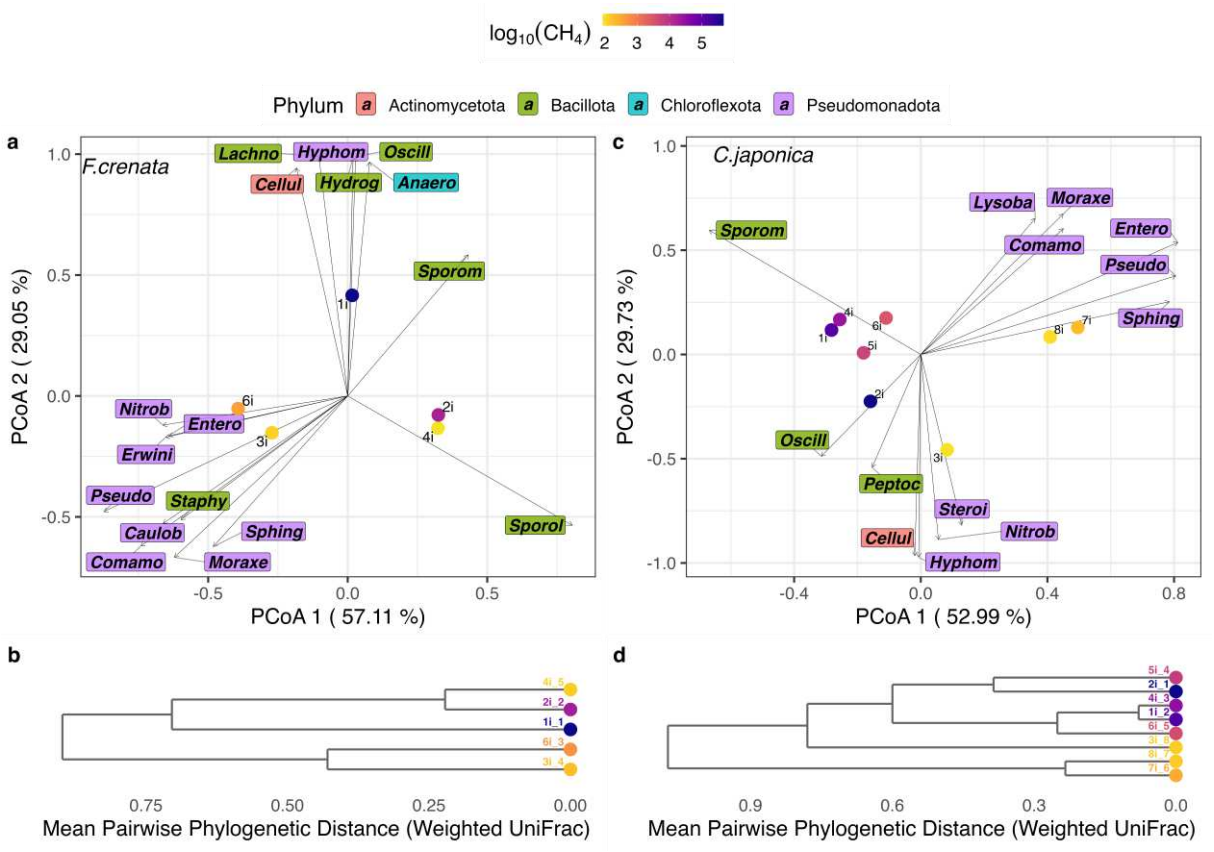
937



938

939 **Figure 5.**

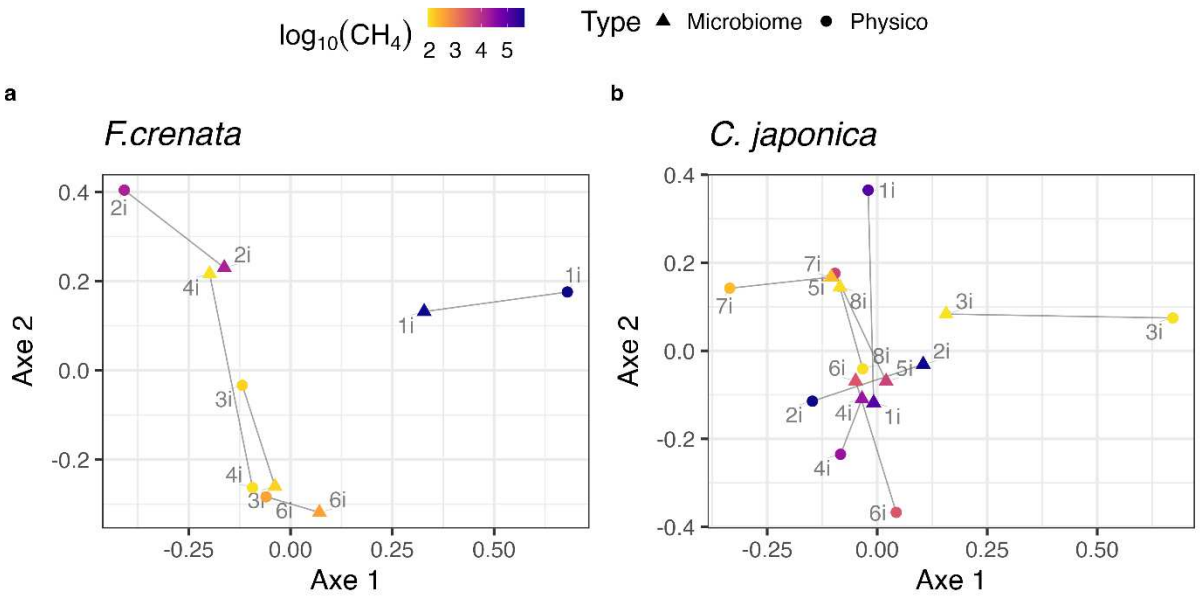
940



941

942 **Figure 6.**

943



944

945 **Figure 7.**

Supplementary Files

This is a list of supplementary files associated with this preprint. Click to download.

- Supplementarymaterial.docx
- TableS2fungiabondanceSI.csv
- TableS3bacterieabondanceSI.csv